Please cite as:
Wenzel, M. N. et al. (2019), "Insights into the Mechanisms of Aquaporin-3 Inhibition by Gold(III) Complexes: the Importance of Non-Coordinative Adduct Formation", Inorganic Chemistry, Vol. 58, N. 3, pp. 2140-2148, doi: https://doi.org/10.1021/acs.inorgchem.8b03233

Insights into the Mechanisms of Aquaporin-3 Inhibition by Gold(III) Complexes: the Importance of Non-Coordinative Adduct Formation

Margot N. Wenzel,[†,‡] *Andreia F. Mósca,*[‖,‡] *Valentina Graziani,*[§,‡] *Brech Aikman,*[†] *Sophie R. Thomas,* [†] *Andreia de Almeida,*[†,¥] *James A. Platts,*[†] *Nazzareno Re,* [§] *Cecilia Coletti,*[§] *Alessandro Marrone,*[§,*] *Graça Soveral,*[‖,*] *Angela Casini* [†,*]

[†] School of Chemistry, Cardiff University, Main Building, Park Place, CF10 3AT Cardiff, United Kingdom.

[‖] Research Institute for Medicines (iMed.ULisboa), Faculty of Pharmacy, Universidade de Lisboa, 1649-003 Lisboa, Portugal.

[§] Università "G. d'Annunzio" di Chieti-Pescara, Department of Pharmacy, Via dei Vestini 31, 66100 Chieti, Italy.

[¥] Tumour Microenvironment Group, Division of Cancer and Genetics, School of Medicine, Cardiff University, Tenovus Building, Cardiff CF14 4XN, United Kingdom

KEYWORDS. Gold complexes; aquaporins; stopped-flow spectroscopy; quantum mechanics/molecular mechanics; molecular dynamics; non-covalent adducts.

ABSTRACT. Following our recent reports on the inhibition of the water and glycerol channel aquaglyceroporin-3 (AQP3) by the coordination complex [Au^{III}(1,10-pehanthroline)Cl_2]

(**Auphen**), a series of six new Au(III) complexes featuring substituted 1,10-phenanthroline ligands (**1-6**) have been synthesized and characterized. The speciation of the compounds studied in buffered solution by UV-Visible spectrophotometry showed that most of the complexes remain stable for several hours. Quantum mechanics (QM) studies of the hydrolysis processes of the compounds suggest that they are thermodynamically less prone to exchange the chlorido ligands with H_2O or OH^- compared to Au(III) bipyridyl complexes. Preliminary data on the antiproliferative activity against A549 human lung cancer cells indicate that the compounds are able to inhibit cell proliferation *in vitro*. Stopped flow spectroscopy showed that these complexes potently inhibit glycerol permeation in human red blood cells (hRBC) through AQP3 blockage. The QM investigation of the ligand exchange with methane thiol, used as a model of Cys40 of AQP3, was carried out for some derivatives, and showed that the affinity of the compounds' binding for thiols is higher compared to the **Aubipy** complex ($[Au^{III}(bipy)Cl_2]PF_6$, bipy = 2,2'-bipyridine). In addition, both non-covalent and coordinative binding of complex **3** $[Au^{III}$(5-chloro-1,10-phenanthroline)$Cl_2]PF_6$ to the protein channel has been investigated in comparison to the benchmark **Auphen** and **Aubipy** using a computational workflow, including QM, molecular dynamics (MD) and quantum mechanics/molecular mechanics (QM/MM) approaches. Finally, Atoms-in-Molecules (AIM) and Natural Bond Orbital (NBO) analyses corroborate the MD predictions providing quantification of the non-coordinative interactions between the compounds and AQP3. AQP3 inhibition is the result of protein conformational changes, upon coordinative gold binding, which induce pore closure. The importance of non-coordinative adducts in modulating the AQP3 inhibition properties of the investigated Au(III) compounds has been elucidated, and these interactions should be further considered in the future design of isoform selective AQP inhibitors.

INTRODUCTION

Cells require membrane channels, the aquaporins (AQPs), to allow fast permeation of water, glycerol and other small solutes, including hydrogen peroxide, across their membranes in response to osmotic gradients [1]. Therefore, these membrane channels are present in most cell types and play crucial roles in human physiology, such as skin hydration and wound healing, fat metabolism and urine concentration [2]. Notably, AQPs have been correlated to cancer biology and development and various different isoforms were shown to be expressed in more than several human cancers and at different stages of the disease [3-4]. Different isoforms have been linked to various tumour types and grades, as well as cancer cellular processes as proliferation, migration and angiogenesis [5-6]. Therefore, these protein channels have been proposed as emerging drug targets for various diseases, including cancer [6-7].

Structurally, AQP channels are very similar: assembled as tetramers in cell membranes, with each monomer forming a hourglass-shaped channel, which is derived from six alpha-helices that span across the cell membrane and two semi-helices that meet at the centre of the protein [8]. The pore's selectivity to various substrates is determined by its specific structural features: a constriction site, 3-4 Å wide, named the aromatic/arginine selectivity filter (ar/R SF), and a second selectivity filter composed of two asparagine-proline-alanine (NPA) motifs, highly conserved in all AQPs. Solute's size-exclusion is generally determined by the size of the ar/R SF, which can vary slightly among AQPs, depending on the exact amino acid composition of this site, while the NPA motifs are responsible for creating a positive dipole moment at the side chains of the two asparagine residues, acting as a barrier for charged species [8 9].

Solute selectivity varies among the 13 mammalian AQPs described so far and three major groups can be identified: i) *orthodox aquaporins* (AQP0, AQP1, AQP2, AQP4, AQP5, AQP6 and AQP8), which are primarily water selective [10], ii) *aquaglyceroporins* (AQP3, AQP7, AQP9 and AQP10), permeable to small uncharged solutes such as glycerol [11] and iii) *superaquaporins*, AQP11 and AQP12, which are permeable to water and glycerol, even though they have lower sequence homology with other AQPs and are located in intracellular membranes [12-13].

Aquaglyceroporins in particular, are known to regulate glycerol content in various tissues, such as epidermis or fat, and their role as a glycerol channel has been proposed to be involved in skin hydration and wound healing, cell proliferation, lipid metabolism and carcinogenesis [2]. However, the involvement of aquaglyceroporins in these physiological processes has been mostly studied using genetically modified organisms. Thus, in order to validate the various roles of AQPs in health and disease, as well as to develop AQP-targeted therapies, the use of selective inhibitors in addition to genetic approaches, holds great promise [7]. However, none of the reported organic small-molecule AQP inhibitors show sufficient isoform selectivity to be seen as suitable candidates for clinical development [7, 14-15].

Recently, Au(III) coordination compounds have been identified as selective aquaglyceroporin inhibitors [16]. In 2012, we were the first to report on the potent and selective inhibition of human AQP3 by a series of Au(III) complexes with nitrogen-donor ligands [17-18]. The compounds could efficiently inhibit glycerol transport through hAQP3 in human red blood cells (hRBC), while they were not active on water transport *via* the orthodox water channel human AQP1 [17]. The most potent inhibitor of the series, **Auphen** ($[Au^{III}(phen)Cl_2]Cl$, phen = 1,10-phenanthroline) had an IC_{50} in the low micromolar range (0.8 ± 0.08 μM) and was far more effective than the benchmark AQPs inhibitor, the mercurial compound $HgCl_2$ [17]. In a subsequent

study, we examined **Auphen** capacity of inhibiting cell proliferation in various cell lines, including cancerous ones, with different levels of AQP3 expression [19]. The obtained results showed a direct correlation between AQP3 expression levels and the inhibition of cell growth by the Au(III) compound. Furthermore, AQP3 inhibition was observed in the cell lines where proliferation was mostly affected by treatment with the gold compound.

In general, the chemical design of innovative and highly selective inhibitors should be supported by structural information on the target AQP protein. When the latter is lacking, as in the case of most human aquaglyceroporins, computational methods are essential tools to obtain the structure-activity relationships, and several homology models have recently been proposed for different AQPs isoforms [20-23]. The use of such models is recommended to achieve a deeper understanding of the key structural features involved in substrate transport, and helpful to improve AQP-targeted drug design. In this context, in the last years, we have conducted a number of studies based on molecular modelling approaches and aimed at the elucidation of the molecular mechanisms of human AQP3 inhibition by gold compounds. Initially, we investigated the non-covalent binding of **Auphen** to AQP3 by molecular docking and observed that the compound's isoform selectivity may be due to the accessibility of Cys40 [17]. The latter is located at the extracellular side of the protein channel and features a thiol group in its side-chain, which is a likely candidate for direct binding to Au(III) complexes. The importance of this residue in the binding of **Auphen** to AQP3 was further confirmed by site-directed mutagenesis studies [19].

More recently, AQP3's inhibition mechanism by **Auphen** has been described by us using molecular dynamics (MD), combined with density functional theory (DFT) [24]. The obtained MD results showed that gold-based inhibitors, anchored to Cys40 in AQP3, are able to induce shrinkage of the pore preventing substrate permeation. This finding has important implications

for future inhibitor design: in fact, other amino acid residues could be targeted, provided that their modification leads to the necessary conformational changes to achieve channel closure. Moreover, the MD studies showed that binding of the gold compound in one monomer also affects substrate permeability in an adjacent one, while altering the overall extracellular distribution of hydrophobic/hydrophilic surfaces of the tetramer, which, in turn, may affect the approach of the substrates to the pore [24].

Further investigation of another selective AQP3 inhibitor, the Au(III) cationic complex **Aubipy** $[Au(bipy)Cl_2]PF_6$ (bipy = 2,2'-bipyridine) (IC_{50} = 2.3 ± 0.7 μM), bound to the protein channel, has been performed by means of a multi-level theoretical workflow including MD and quantum mechanics/molecular mechanics QM/MM approaches [25]. Thus, the structures of both non-covalent and covalent (Cys-bound) **Aubipy**-AQP3 adducts were studied through the use of classical MD simulations to gain a detailed insight into the **Aubipy** binding and its consequences on the AQP3 functionality. In this study, three key aspects for AQP3 inhibition by gold compounds emerged: i) speciation of the Au(III) complex prior to protein binding (formation of aquo-complexes), ii) stability of non-covalent adducts between the compound aromatic ligand and the extracellular pore side, and iii) protein conformational changes upon coordinative binding of Au(III) ions leading to pore closure, in line with the above-mentioned study on **Auphen**.

Considering that **Auphen** structure is one of the most effective in inhibiting glycerol permeation via AQP3 in hRBC and, in order to optimize the compound's scaffold to improve the protein binding and to achieve structure-activity relationships, we have synthesized a new series of six Au(III) complexes in which the phenanthroline ligand has been derivatized at different positions (**1-6**, Scheme 1). The compounds have been studied for their AQP3 inhibition

properties in hRBC by stopped-flow spectroscopy and evaluated for their anticancer properties against the human lung cancer cells A549 *in vitro*. Initially, the speciation of the gold complexes was studied by Quantum Mechanics (QM) calculations in comparison to **Auphen** and **Aubipy**. The QM investigation of the ligand exchange reaction with methane thiol, used as a model, was carried out for **Auphen** and complexes **2-4**. Intrigued by the role of non-covalent with respect to covalent metallodrug-AQP3 adducts in the inhibition mechanisms of **Auphen** and analogues, we applied molecular dynamics (MD) simulations to further explore the system at a molecular level for **3** in comparison to **Auphen**. Non-covalent interactions that lead to binding of **Auphen** and **3** to AQP3 were further probed using Atoms-in-Molecules (AIM) and Natural Bond Orbital (NBO) analysis. Overall, while the Auphen-type complexes feature similar mechanism of AQP3 inhibition, important differences were evidenced with respect to the bipyridyl complex **Aubipy**, in line with the observed variations in the experimental inhibition potency of the compounds.

RESULTS AND DISCUSSION

Synthesis and Characterization

The synthesis of a series of Au(III) phenanthroline-based complexes **1-6** was achieved by coordination reaction of phenanthroline derivatives functionalized in various positions with different functional groups (methyl, phenyl, chloro, nitro) with a Au(III) precursor (Scheme 1). Some of the Au(III) complexes (**2**,[26-27] **4** [28-30] and **6** [27, 29]) were already described in the literature, but with different counter ions other than PF_6. All the chosen phenanthroline ligands were commercially available. The formation of the Au(III) complexes proceeds in one step by reaction between 1 eq. of phenanthroline ligand dissolved in acetonitrile and 1 eq. of Au(III) precursor

salts ($NaAuCl_4$ or $KAuCl_4$) dissolved in water with an excess (3 eq.) of KPF_6. The reactions were complete in a few hours at reflux with precipitation of the product. The obtained pale to dark yellow powders were then characterized by multinuclear 1D and 2D NMR spectroscopy (See Experimental Section and Supplementary Information Figures S1-S18), high-resolution mass spectrometry, UV-Visible and infrared spectroscopies. Notably, interpretation of the ^{1}H NMR spectra of all the complexes confirmed the coordination of the phenanthroline derivatives to the Au(III) ion as a downfield shift of up to 0.7 ppm was noticed for all proton signals of the complexes in comparison with the initial ligands. ^{31}P and ^{19}F NMR spectra also confirmed the presence of the PF_6^- counter ion in the final products, with the presence of a doublet and a heptuplet in ^{19}F and ^{31}P NMR spectra, respectively.

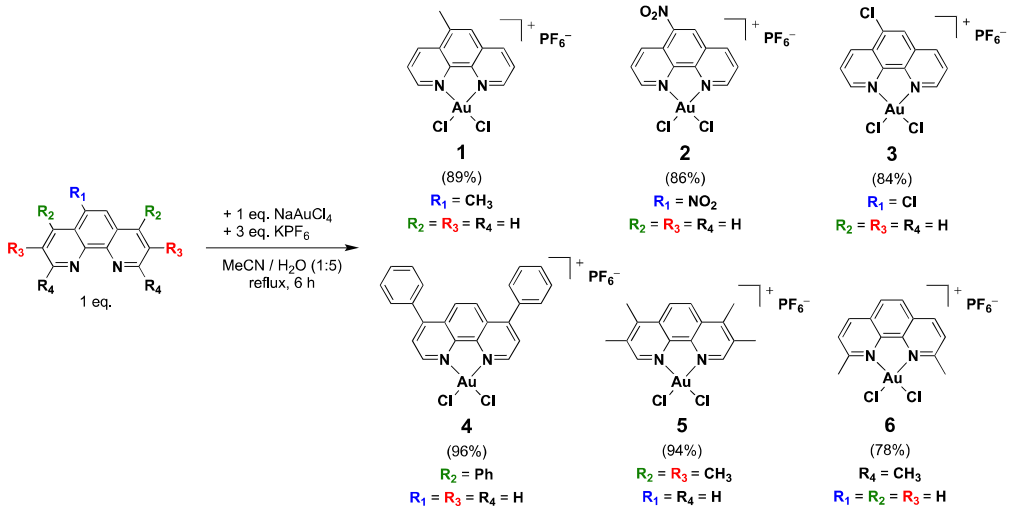

Scheme 1. General scheme for the synthesis of complexes **1-6** and related yields.

Stability in physiological medium

Initially, the stability of the new gold complexes **1-6** was evaluated by UV-Visible spectroscopy. In parallel, as Au(III) complexes tend to be reduced in physiological conditions to

Au(I) and even Au(0) [31], a similar experiment was conducted under the same conditions and with addition of 2 eq. of the, physiologically relevant reducing agent, glutathione (GSH) per equivalent of Au(III) complex. Thus, the absorbance of the solutions was measured between 275 and 700 nm at regular time intervals during 24 h at room temperature, allowing the monitoring of possible transformations such as hydrolysis, reduction and/or precipitation of the complexes. The results are shown in Figures S19-S24 in the supplementary material. All six complexes exhibit intense transitions in the 300-400 nm range, characteristic of the Au(III)-containing chromophore, that may be straightforwardly assigned as LMCT (Ligand to Metal Charge Transfer) bands. In these cases, spectral changes are observed with time that might be related to the occurrence of partial hydrolysis processes of the chlorido ligands. Instead, spectra of complexes **4** and **6** show a marked decrease in intensity of the LMCT bands characteristic of the Au(III) phenanthroline chromophore (Figures S22 and S24), which in both cases goes in parallel to the formation of a precipitate. We hypothesize that initially hydrolysis of the chlorido ligands takes place as for the other derivatives, followed by reduction of the Au(III) centre to Au(I) or Au(0). However, formation of colloidal gold could not be observed in all cases, which should have resulted in the appearance of a broad absorption band around 550 nm. Further characterization of the insoluble products should be achieved to exclude possible Au(III) reduction processes and to fully characterize the pathways to such extensive decomposition.

Aquaporin inhibition

The compounds were tested for their ability to inhibit AQP1 and AQP3 by stopped flow spectroscopy using human red blood cells (hRBC), as described previously [17]. All the complexes showed to selectively inhibit AQP3 glycerol permeability P_{Gly}, with IC_{50} values in the sub-micromolar level, being similar or even lower than **Auphen** (Table 1). As expected, the tested

compounds did not show any inhibitory effect on AQP1 water permeability, as previously reported for **Auphen** (data not shown). The most potent inhibitory effect was detected for complexes featuring substituents in position 5 of the phenanthroline ligand, with compound **4** being the most active (IC_{50} of 0.43 ± 0.08 μM) followed by **2** and **3**, as represented in Figure 1.

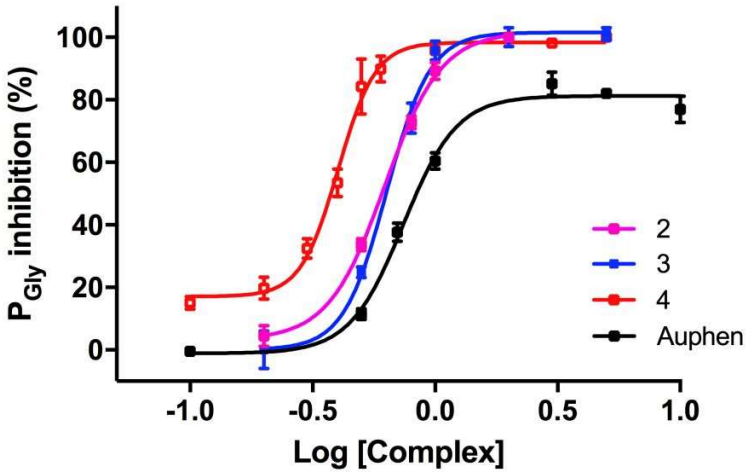

Figure 1. Representative IC_{50} curve for the inhibition of glycerol permeation of AQP3 by the Au(III) complexes **Auphen** and **2-4**.

Table 1. Glycerol permeation inhibiting effects (IC_{50} values) of various Au(III)-phenanthroline complexes (**Auphen**, **1-6**) and the Au(III) bipyridine complex **Aubipy** in hRBC after 30 min incubation. N = number of independent experiments.

Complex	IC_{50} (μM)[a]
Auphen	0.80 ± 0.08
Aubipy	2.3 ± 0.7
1	0.73 ± 0.09
2	0.57 ± 0.04 (N = 2)
3	0.57 ± 0.07 (N=2)
4	0.43 ± 0.08
5	0.83 ± 0.01 (N=1)

6	0.89 ± 0.14

[a] Values represented as mean ± SEM of at least three independent experiments, unless otherwise stated.

Antiproliferation assays

The antiproliferative properties of complexes **1-6** were evaluated using the classical MTT [3-(4,5-dimethylthiazol-2-yl)-2,5-diphenyltetrazolium bromide] assay, after 72 h of treatment, against the human lung cancer cell line A549, which expresses AQP3 [32]. Overall, the complexes displayed strong antiproliferative properties, with EC_{50} values in the low micromolar range (Table S1). Specifically, complexes **4** and **5** were found as potent as the benchmark **Auphen** with EC_{50} values of ca. 1 μM. The ligands induced antiproliferative effects similar to their corresponding complexes (Table S2), in line with previously reported results [33-34], suggesting that the observed effect of the complexes could also be due to the release of ligand itself over time. Thus, the obtained results may suggest that the compounds are not ideal for further development as anticancer agents, unless the control of their speciation will be achieved (e.g. *via* the use of drug delivery systems). Nevertheless, the Au(III) complexes could still be used as chemical probes to study AQP3 function in cells benefiting of their isoform selectivity.

Correlation of AQP3 inhibition with DFT-calculated properties of Au(III) compounds

The structural features of **Auphen** and **1-6** complexes, expected to exert a major control on their reactivity with Cys40 side chain (i.e. presumed to be their coordinative binding site on AQP3) were calculated by means of DFT approaches. Indeed, the HOMO-LUMO gap and the charge on the Au metal center are connected to the orbital and charge control, respectively, in the

reaction with nucleophiles. Thus, modulation of these electronic factors may be exerted by the presence of different substituents on the phen scaffold. The correlation of glycerol permeation activity as $\log_{10}(1/IC_{50})$ with DFT-calculated properties of Au(III) complexes was then examined, including the energy of frontier orbitals (E_{HOMO} and E_{LUMO}) and their difference (E_{gap}), the partial charge on metal center (q(Au)), as well as the molecular dipole and volume (Table S3). In general, a poor correlation between calculated properties and experimental data was detected (Table S4), although we noticed a slightly higher correlation of $\log_{10}(1/IC_{50})$ with qAu, dipole, and volume compared to the other properties. However, it seems clear that the dependence of *in vitro* activity on molecular structure is not straightforward, prompting us to carry out more detailed calculations on speciation and binding to potential biological targets.

Speciation Study by Quantum Mechanics

The speciation of gold complexes was further studied by QM calculations. Specifically, investigation of the aquation processes of the most active complexes as AQP3 inhibitors, namely **2**, **3** and **4**, was carried out by using the computational procedure and decomposition scheme described elsewhere [25], and compared with those of **Auphen** and **Aubipy** (see Experimental section for details). The obtained results showed that, as already stated for **Aubipy** [25], the speciation of Auphen-like species is determined by a hydrolysis process followed by diffusion-controlled and quantitative deprotonation of the bound water molecules – negative free energy values (Table 2) – leading to only three possible species in water solution: dichloro, chloro-hydroxo, and dihydroxo species. The estimation of both reaction and activation free energies was carried out by decomposing these processes as depicted in Scheme 2. The calculated activation free energy for either first or second aquation of the Auphen-like complexes resulted to be quite

similar to that of **Aubipy**, with the highest difference in the order of 5 kJ/mol (Table 2). However, such differences are within the accuracy limit expected for density functional theory estimation of activation barriers (about 8 kJ/mol). Therefore, our computational model indicates a similar hydrolysis rate for all considered Au(III) complexes. The only exception is represented by the appreciably lower activation free energy for the second aquation of **4**, caused by the particularly low free energy contribution for step 1 (Scheme 2), i.e. –0.8 kJ/mol which is about 30 kJ/mol less compared to the other Auphen-like complexes.

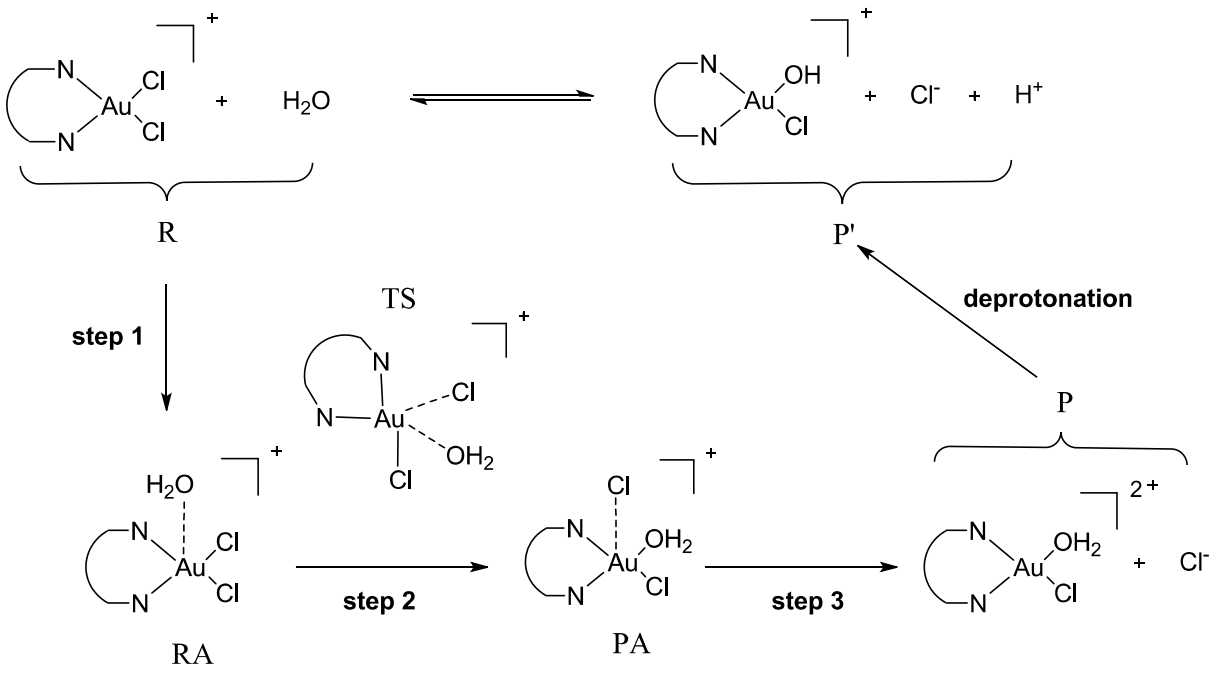

Scheme 2. Reaction decomposition scheme for the hydrolysis of one of the chlorido ligands in **Auphen**, *i.e.* first aquation. R = reactants, RA = reactant adduct, TS = transition state, PA = product adduct, P and P' = products before and after deprotonation, respectively.

Table 2. Reaction free energy parameters for the first (I) and second (II) aquation of Au(III) complexes. All values in kJ/mol.

Complex	ΔG_I^0	ΔG_{II}^0	$\Delta G_I^{\ddagger}$	$\Delta G_{II}^{\ddagger}$
Aubipy	44	63	118	103
Auphen	77	86	124	126
2	67	87	117	121
3	73	84	122	124
4	77	57	122	94

On the other hand, calculations indicated that both first and second aquation of Auphen-like complexes are thermodynamically less favored than **Aubipy** (Table 2). The overall reaction free energy for the first and second aquation of **Auphen** is higher by 23 and 20 kJ/mol, respectively, and such differences are essentially maintained in the case of the other Auphen-like scaffolds. The only exception is represented by the second aquation of **4,** which is conversely 10 kJ/mol lower in comparison with **Aubipy**. It is worth mentioning that the estimated thermodynamic constants for the first and second aquation of the gold complexes were calculated assuming to be in water, at pH 7.4 ($[H^+] = 3.98\times10^{-8}$ M) and a constant chloride concentration ($[Cl^-]$ = 100 mM). Therefore, according to the obtained results, we can infer that, in physiological conditions, the Auphen-like complexes are prevalently in the dichloro form, presumed to bind at the extracellular pore of AQP3. This result highlights a significant difference with respect to **Aubipy**, the latter having been predicted to bind AQP3 in the corresponding chloro-hydroxo form [25].

The decomposition of the calculated standard free energy values for either **Aubipy** and **Auphen** first aquation evidenced that the only significant difference between these complexes is detected on step 2 (Scheme 2) which is 26 kJ/mol more endergonic for **Auphen** (Scheme 3). By

breaking down step 2 energy it is clearly evidenced that this value is gained by the summation of a positive gas phase term plus a negative solvation term in both **Aubipy** and **Auphen**. In fact, in spite of the less favorable gas phase term, the solvation term in **Aubipy** is much lower than in **Auphen**, i.e. by about -52 kJ/mol, thus making step 2 of **Auphen** aquation more endergonic (Table S5).

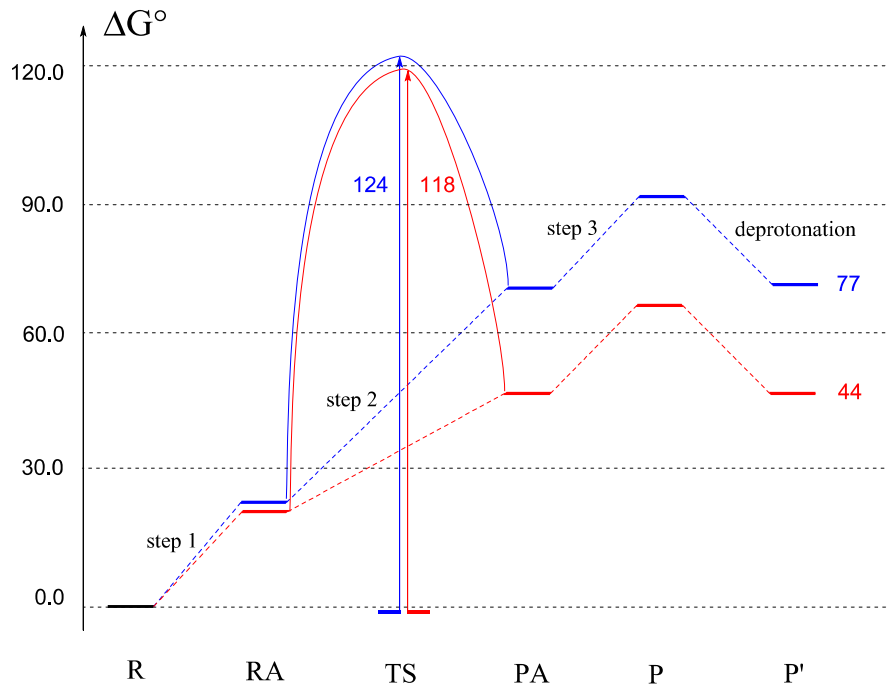

Scheme 3. Free energy profiles of the first aquation (I) of **Aubipy** (red) and **Auphen** (blue). All values in kJ/mol.

Quantum Mechanics Study of Binding to Thiols

To further investigate why the gold complexes have different AQP3 inhibitory effects, and assuming Cys40 as the gold binding site as in the case of **Auphen**, the QM investigation of the ligand exchange with methane thiol, used as a model, was carried out for **Auphen** and complexes **2-4**, all reacting in the corresponding dichlorido form. The decomposition scheme employed for aquation (Scheme 2) was similarly applied to the substitution of chloride with

thiol; thus, the same thermodynamics and kinetics parameters were calculated. The overall activation free energy ($\Delta G^{\ddagger}_{obs}$), as well as free energy values for either pre-equilibrium of reactant adduct (RA) formation (ΔG^{0}_{step1}) or barrier from RA to PA ($\Delta G^{\ddagger}_{step2}$), of Cl^- substitution with methane thiol for **Auphen** and **3** are essentially the same estimated for **Aubipy**, with differences within the expected theoretical accuracy. On the other hand, the activation free energies for the reaction with thiol of complexes **2** and **4** were lower by about 10-15 kJ/mol (Table S6). In all cases, the pre-equilibrium for the formation of RA is endergonic, thus contributing to increase the kinetic barrier for chloride substitution, and characterized by free energy values in the narrow range of 29-40 kJ/mol. As already reported for **Aubipy**, [25] the free energy loss for the formation of RA could be compensated by the non-coordinative interactions between the gold complex and AQP3 residues, thus, kinetically favoring its coordination at the thiol moiety of Cys40 residue. Interestingly, the free energy values for the thiol/Cl^- exchange of **Auphen** and complexes **2-4** were lower than the corresponding value for **Aubipy**, thus, indicating that the coordination to thiolate is more favored in the Auphen-like complexes. This result is in good agreement with the higher glycerol permeation inhibition disclosed by Auphen-like compounds ascribable to a higher amount of covalently bound AQP3 units compared to **Aubipy**, when equilibrium is reached.

Molecular dynamics (MD) simulations of the binding to AQP3

In order to further corroborate the above-mentioned hypothesis of the importance of non-covalent interactions to determine the selectivity of AQP3 binding by gold complexes, we applied classical MD simulations to further investigate the gold complex/protein adduct. The quaternary structure of AQP3 was prepared *via* homology modelling, following an approach

previously described by us and reported in the Experimental section [24-25]. Thus, both non-coordinative and coordinative adducts of **Auphen** and of one of the most active inhibitors, the 5-subsituted-chloro-phenanthroline complex **3** (IC_{50} = 0.57 ± 0.07 μM), with AQP3 were simulated in the Amber force field to sample a set of representative configurations of each system. The obtained results were compared with the previously reported ones for **Aubipy** [25].[25] This approach evidenced the effects of varying the nitrogen donor ligand scaffold (from phen to bipy) on the AQP3-binding mode of the Au(III) complexes, as well as the effects of the substitution in position 5 of the phen ligand.

The input structures of either NCA or CA structure of **Auphen** and **3** were obtained *via* superimposition of metal center on the corresponding **Aubipy**-AQP3 complexes. The representative conformations obtained by the end of the workflow encode the structural features disclosed by the system, including the effects of thermal motion, and allowed to significantly enhance the *a posteriori* QM analyses of the electronic structure of non-coordinative adducts (*vide infra*). The coordinative adducts of both **Auphen** and **3** displayed geometrical parameters that resemble the corresponding structures of the **Aubipy**-AQP3 system, although some differences between **Auphen** and **3** were unveiled (Figure 2). Specifically, **Auphen** is slightly more buried inside the pore than **3**. This feature allowed establishing a T-shape contact of the phen moiety of **Auphen** with Phe63, which was not detected in the case of **3**. The water exposure of the two compared scaffolds is also slightly different, with **Auphen**, in analogy to **Aubipy**,[25] exposing only one ring to the solvent, while **3** is exposing a larger portion, i.e. one pyridyl ring plus middle phen ring (Figure 2).

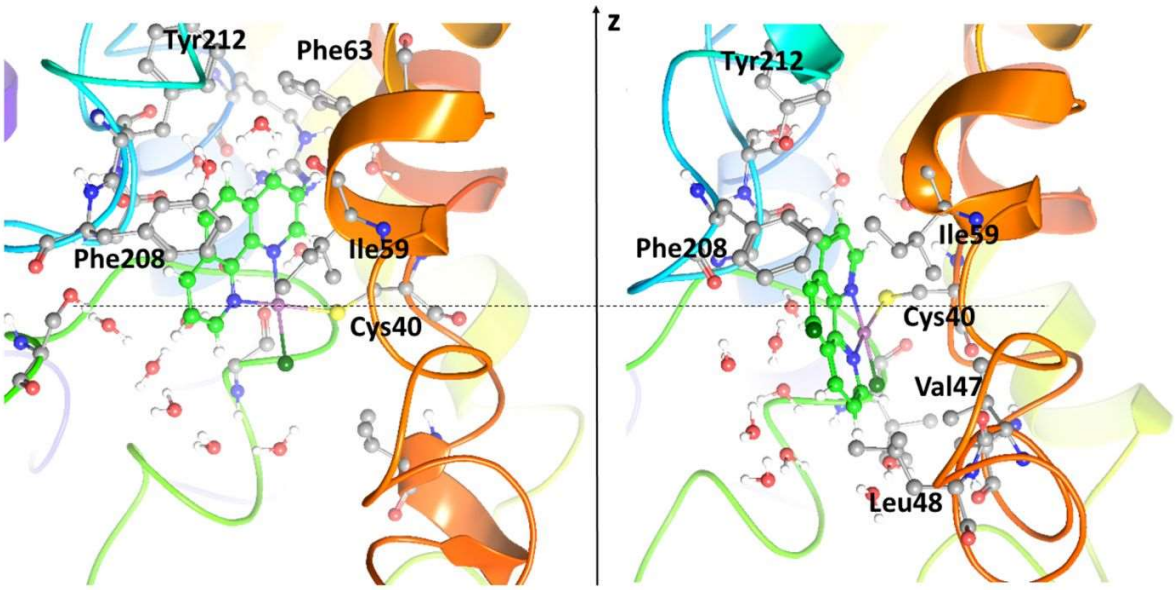

Figure 2. Most representative coordinative adducts of either **Auphen** (left) or the [(5-chloro-1,10-phenanthroline)$AuCl_2$]$^+$ complex (**3**) (right) with AQP3, as seen from the extracellular side. The positions of Cys40 sulfur atom along the z-axis are labeled (black dashed lines). Metal complex and protein carbons are represented in ball-and-stick and colored green and gray, respectively.

A similar impact on both shape and functionality of the AQP3 was evidenced by the analysis of **Auphen** and **3** coordinatively bound complexes. Both adducts compared similarly with the corresponding **Aubipy** system, showing a decrease of the simulated water flux (Table S7). The observed decrease of water permeation is caused by conformational rearrangements occurring on the side of proximal residues upon the coordinative binding of the gold moiety, in line with previously reported studies for another Au(III) complex [24]. In particular, the side chain of Arg218, forming the selectivity filter (ar/R SF) of AQP3, adopts a folded conformation in the coordinative complex, while being much more flexible in the unbound AQP3, as elsewhere reported for **Aubipy** [25]. Indeed, rather strong hydrogen bond interactions between the guanidine group of Arg218 and the AQP3 backbone were detected in both **Auphen** and **3** coordinative complexes (Scheme 4).

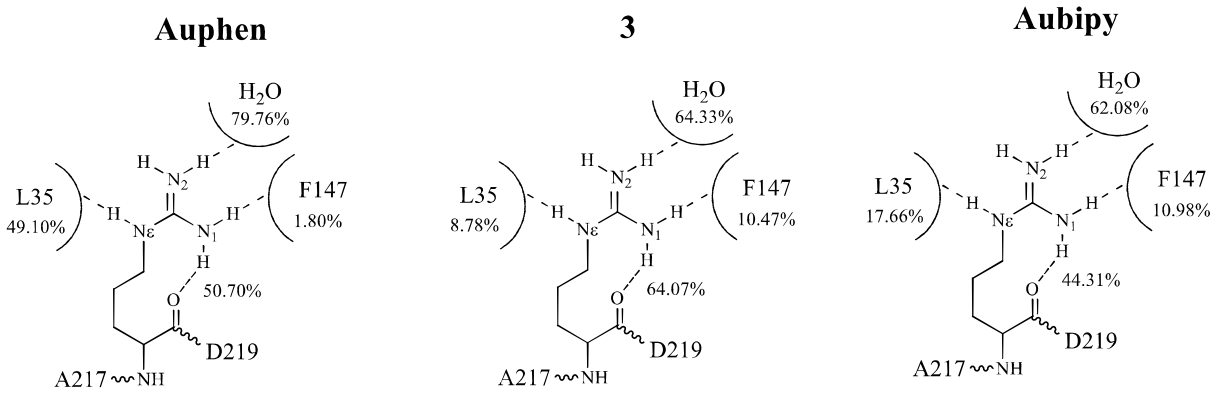

Scheme 4. A sketch of the hydrogen bond pattern of Arg218 obtained by MD simulation of **Auphen**, **3** and **Aubipy** [25] coordinative adducts with AQP3. The percentages of trajectory in which tiled hydrogen bonds exist are also reported.

MD simulation of the non-coordinative adducts of **Auphen** and **3** were also performed. Both metal complexes were initially placed to resemble the binding pose of the corresponding **Aubipy**-AQP3 complex through the superimposition of phen to the bipy moiety of **Aubipy** reported by Graziani et al., and by assuming both **Auphen** and **3** to interact via π-π stacking between their metallacycle and the phenyl ring of Phe136 [See structure B1 in ref. [25]]. Notably, while **Auphen** maintained approximately the starting position, compound **3** essentially detached to find interaction with AQP3 outside the extracellular entrance of the pore (data not shown). Based on this outcome, the starting pose of compound **3** was changed by a 180° rotation along an axis passing through the two pyridyl nitrogens, and MD simulation was carried out. In this new initial orientation, compound **3** roughly maintains its starting position and forms a non-coordinative complex with AQP3 that resembles the one formed by **Auphen**. The most representative poses of both **Auphen** and **3** non-coordinative adduct with AQP3 are compared in Figure 3. The results show the two gold complexes interacting with residues at the edge of the

extracellular pore of AQP3. In this pose, the compounds are on average 11.17 and 11.36 Å (Au-S) apart from Cys-40 (Table S8), which is by 3 Å shorter than the one detected in the **Aubipy**-AQP3 adduct [25]. This slightly closer approach to the final coordinative site is in agreement with the higher potency of either **Auphen** or **3** compared to **Aubipy**, and it is probably connected to the lower hydrophilicity of the $AuCl_2$ moiety that in these complexes is projected inside, i.e. towards the Cys40 position. In fact, MD calculations indicate that the complexes interact differently with the surrounding AQP3 residues. The **Auphen** scaffold is involved in stacking interactions with the phenyl ring of both Phe136 and Phe208, whereas compound **3** appears to interact with Phe208 and Asn141 mostly through the metal center: the phenyl ring of Phe208 is placed within 4 Å from Au, amenable for a π-metal interaction, while the backbone C=O of Asn141 is placed with oxygen at only 3.0 Å, thus, amenable for an apical interaction with the positive charge on gold (Figure 3).

Overall, the MD calculations indicate that **Auphen** and its chloro-derivative **3** are both able to form similar coordinative adducts with AQP3 and give rise to similar alterations of the channel structure and functionality. Moreover, these species form stable non-coordinative adducts with AQP3 mainly through the formation of stacking interactions, although, compared to **Aubipy**, the detected poses of **Auphen** and **3** appear to be more amenable for the further reaction with Cys40.

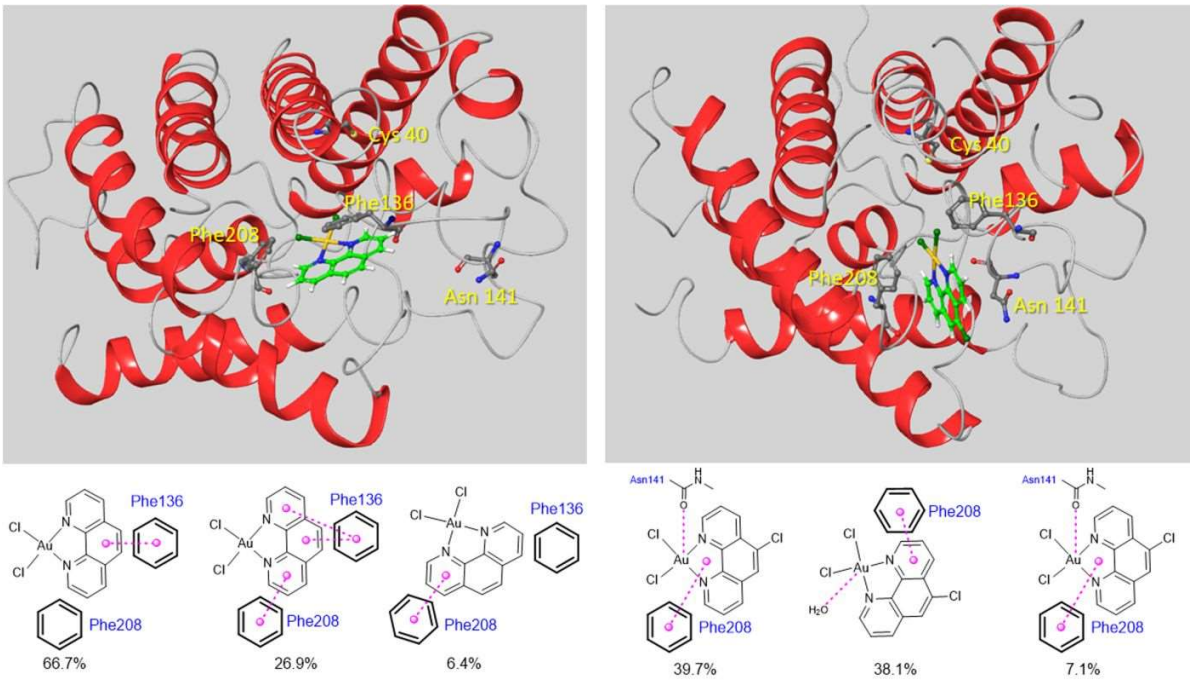

Figure 3. Representation of non-coordinative adducts (the most representative pose) of **Auphen** (left) and **3** (right) with AQP3 (top). 2D sketches of main non-coordinative interactions detected and weights (percentages) of representative poses: the phenyl ring of either Phe136 or Phe208 are bold sketched to highlight that they are placed over the phen scaffold.

Non-covalent interactions that lead to binding of **Auphen** and **3** to AQP3 were further probed using Atoms-in-Molecules (AIM) and Natural Bond Orbital (NBO) analysis. Representative structures obtained after clustering were minimized using QM/MM, then truncated by selecting all amino acids with at least one atom within 3.5 Å. These structures were used to carry out DFT single point calculations, the electron density of which was searched for bond critical points corresponding to direct contacts between metal complex and amino acids. Two **Auphen** clusters (denoted **Auphen.1** and **Auphen.2**) account for over 90% of frames: **Auphen.1** exhibits two bond critical points (BCPs) corresponding to stacking of the phen ligand with each of Phe136 (ρ_c = 0.006 and 0.004 au) and Phe208 (both 0.004 au). We also find BCPs for C—H…O contacts with backbone of Phe136 and Gly142 (0.004 and 0.007 au, respectively),

and for C—H…Cl contacts with Phe208 (0.004 x 2 and 0.002 au). **Auphen.2** is similar, with BCPs for stacking with Phe136 (0.005 au) and Phe208 (0.004 and 0.003), as well as C—H…O interactions with Phe136 (0.004 au) and Phe208 (0.007 au), and C—H…Cl contacts with Val43 (0.007 and 0.006 au), Phe208 (0.006 and 0.004 au). A single C—H…N contact with His154 is also present (0.007 au). In the case of compound **3**, two clusters (denoted **3.1** and **3.2**) account for *ca.* 80% of the trajectory. For **3.1**, contacts to the phen ligand include π-stacking to Phe208 (ρ_c = 0.008 au) and C—H…π to Cβ of Asn141 (0.004 au), along with Au…O=C_{Asn141} (0.010 au). Phe208 also forms stacking interactions with phen in **3.2**, two critical points (ρ_c = 0.004 and 0.002 au) are located, along with a C—H…Cl—Au contact (0.004 au). A C—H…Cl—Au contact (0.004 au) is also present with Val47, along with two C—H…O interactions with backbone O=C of Tyr150.

NBO analysis allows estimate of the strength of these non-covalent interactions through second-order perturbation analysis. In **Auphen.1**, stacking to Phe136 (1.8 kcal/mol) and Phe208 (2.71 kcal/mol) dominates, with lesser contributions from Gly142 and Gly145 (1.2 and 0.8 kcal/mol). Interactions are rather stronger in **Auphen.2**, Phe136 and Phe208 contributing 4.2 and 4.4 kcal/mol, respectively. Val43 also contributes to binding at 2.9 kcal/mol, as does His154 at 1.4 kcal/mol. Non-covalent binding in **Auphen.1** is predicted to be markedly weaker (6.5 kcal/mol) than in **Auphen.2** (12.8 kcal/mol). For **3**, NBO indicates that in **3.1** the Au…O=C_{Asn141} interaction contributes 11.2 kcal/mol to the non-covalent binding, while π-stacking to Phe208 contributes 12.7 kcal/mol. In **3.2**, stacking to Phe208 gives 4.4 kcal/mol of interaction, while Tyr150 contributes 2.7 kcal/mol to binding. NBO and AIM analyses corroborate the MD predictions by providing for quantification of the non-coordinative interactions between **Auphen** or complex **3** and the residues of AQP3 extracellular pore.

CONCLUSION

In this study, we combined biophysical techniques with advanced computational methods to elucidate the mechanism of inhibition of AQP3 by Au(III) complexes with phenanthroline ligands at a molecular/atomic level. Thus, a new series of six Au(III) complexes featuring phen ligands derivatized at different positions was synthesized and characterized for their stability in aqueous solution and for their anticancer effects *in vitro*. Inhibition of glycerol permeation *via* AQP3 was assessed for each Au(III) compound in hRBC by stopped-flow spectroscopy. Some of the new derivatives showed AQP3 inhibition properties which outperformed the benchmark compounds **Auphen** and **Aubipy**. Our calculations evidenced how the examined Auphen-like complexes and **Aubipy** share several binding properties, although a few relevant differences were unveiled. According to QM studies, in physiological conditions, Auphen-like compounds are stable in the dichloro form while, as previously ascertained,[25] **Aubipy** is prevalently in the form of chloro-hydroxo. This different speciation mostly affects the non-coordinative interaction with AQP3. In fact, both **Auphen** and **3** bind at the extracellular pore side similarly to **Aubipy**, but accessing different residues and with a different orientation. Although the non-coordinative interaction energy is about 40 kJ/mol in either cases, Auphen-like complexes project their metal moiety towards the side chain of the gold binding site Cys40, and at a shorter distance compared to **Aubipy**. This observation indicates that these compounds can more easily reach their final coordinative site. This evidence is also consistent with the higher inhibition of glycerol permeation by **Auphen** and **3** with respect to **Aubipy**. Combined MD-QM/MM corroborated this view. Furthermore, our results show that both **Auphen** and **3** form coordinative adducts with AQP3 that are structurally similar to the one formed by **Aubipy**, inducing protein conformational

rearrangements – as particularly evidenced by the hydrogen bond pattern of the Arg218 side chain – which eventually lead to pore closure (AQP3 inhibition). Overall, our results constitute an important basis for the future design of gold-based inhibitors selectively targeting different AQPs isoforms.

EXPERIMENTAL SECTION

The experimental section of this paper can be found in the supplementary information available and includes general information, synthesis and characterization of the Au(III) complexes, protocols of UV-Visible spectroscopy, aquaporin inhibition studies by stopped-flow spectroscopy and antiproliferative assays. In addition, information on DFT studies, MD and QM/MM calculations are provided.

ASSOCIATED CONTENT

Supporting Information. The supporting information, including NMR spectra of the reported compounds (Figures S1-S18), stability studies by UV-Visible spectroscopy (Figures S19-S24), antiproliferative data (Tables S1-S2) and computational data (Tables S3-S9, Figure S25), is available free of charge on the ACS Publications website at DOI: XXXX.

AUTHOR INFORMATION

Corresponding Authors

*Prof. Angela Casini and Prof. Graça Soveral.

A.C.: School of Chemistry, Cardiff University, Main Building, Park Place, CF10 3AT Cardiff, United Kingdom. Email: casinia@cardiff.ac.uk

G.S.: Research Institute for Medicines (iMed.ULisboa), Faculty of Pharmacy, Universidade de Lisboa, 1649-003 Lisboa, Portugal. Email: gsoveral@ff.ulisboa.pt

A.M.: Università "G. d'Annunzio" di Chieti-Pescara, Department of Pharmacy, Via dei Vestini 31, 66100 Chieti, Italy. Email: amarrone@unich.it

Author Contributions

The manuscript was written through contributions of all authors. All authors have given approval to the final version of the manuscript. ‡These authors contributed equally.

ACKNOWLEDGMENT

Cardiff University and Fundação para a Ciência e Tecnologia, Portugal (project PTDC/BTM-SAL/28977/2017 and PhD fellowship to A.M. SFRH/BD/52384/2013) are acknowledged for funding. A.C. acknowledges support from Cardiff University and the Hans Fischer Senior Fellowship of the Technical University of Munich – Institute for Advanced Study, funded by the German Excellence Initiative and the European Union Seventh Framework Program, under grant agreement n° 291763.

REFERENCES

1. Soveral, G.; Nielsen, S.; Casini, A., *Aquaporins in Health and Disease. New Molecular Targets for Drug Discovery*. 1st Edition ed.; CRC Press: Boca Raton, 2016; p 356.
2. Verkman, A. S., Aquaporins in clinical medicine. *Annu Rev Med* **2012,** *63*, 303-16.
3. Verkman, A. S.; Hara-Chikuma, M.; Papadopoulos, M. C., Aquaporins--new players in cancer biology. *J Mol Med (Berl)* **2008,** *86* (5), 523-9.

4. Ribatti, D.; Ranieri, G.; Annese, T.; Nico, B., Aquaporins in cancer. *Biochim Biophys Acta* **2014,** *1840* (5), 1550-3.
5. Nico, B.; Ribatti, D., Aquaporins in tumor growth and angiogenesis. *Cancer Letters* **2010,** *294* (2), 135-138.
6. Aikman, B.; de Almeida, A.; Meier-Menches, S. M.; Casini, A., Aquaporins in cancer development: opportunities for bioinorganic chemistry to contribute novel chemical probes and therapeutic agents. *Metallomics* **2018,** *10* (5), 696-712.
7. Verkman, A. S.; Anderson, M. O.; Papadopoulos, M. C., Aquaporins: important but elusive drug targets. *Nature reviews. Drug discovery* **2014,** *13* (4), 259-77.
8. Jung, J. S.; Preston, G. M.; Smith, B. L.; Guggino, W. B.; Agre, P., Molecular structure of the water channel through aquaporin CHIP. The hourglass model. *J Biol Chem* **1994,** *269* (20), 14648-14654.
9. Hub, J. S.; de Groot, B. L., Mechanism of selectivity in aquaporins and aquaglyceroporins. *Proc Natl Acad Sci U S A* **2008,** *105* (4), 1198-203.
10. Agre, P., The aquaporin water channels. *Proc Am Thorac Soc* **2006,** *3* (1), 5-13.
11. Hara-Chikuma, M.; Verkman, A. S., Physiological roles of glycerol-transporting aquaporins: the aquaglyceroporins. *Cell Mol Life Sci* **2006,** *63* (12), 1386-92.
12. Ishibashi, K.; Tanaka, Y.; Morishita, Y., The role of mammalian superaquaporins inside the cell. *Biochim Biophys Acta* **2014,** *1840* (5), 1507-12.
13. Madeira, A.; Fernandez-Veledo, S.; Camps, M.; Zorzano, A.; Moura, T. F.; Ceperuelo-Mallafre, V.; Vendrell, J.; Soveral, G., Human aquaporin-11 is a water and glycerol channel and localizes in the vicinity of lipid droplets in human adipocytes. *Obesity* **2014,** *22* (9), 2010-7.
14. Beitz, E.; Golldack, A.; Rothert, M.; von Bülow, J., Challenges and achievements in the therapeutic modulation of aquaporin functionality. *Pharmacol Ther* **2015,** *155*, 22-35.
15. Soveral, G.; Casini, A., Aquaporin modulators: a patent review (2010-2015). *Expert opinion on therapeutic patents* **2017,** *27* (1), 49-62.
16. de Almeida, A.; Soveral, G.; Casini, A., Gold compounds as aquaporin inhibitors: new opportunities for therapy and imaging. *MedChemComm* **2014,** *5* (10), 1444-1453.
17. Martins, A. P.; Marrone, A.; Ciancetta, A.; Galán Cobo, A.; Echevarría, M.; Moura, T. F.; Re, N.; Casini, A.; Soveral, G., Targeting Aquaporin Function: Potent Inhibition of Aquaglyceroporin-3 by a Gold-Based Compound. *PLOS ONE* **2012,** *7* (5), e37435.
18. Martins, A. P.; Ciancetta, A.; de Almeida, A.; Marrone, A.; Re, N.; Soveral, G.; Casini, A., Aquaporin Inhibition by Gold(III) Compounds: New Insights. *ChemMedChem* **2013,** *8* (7), 1086-1092.
19. Serna, A.; Galán-Cobo, A.; Rodrigues, C.; Sánchez-Gomar, I.; Toledo-Aral, J. J.; Moura, T. F.; Casini, A.; Soveral, G.; Echevarría, M., Functional Inhibition of Aquaporin-3 With a Gold-Based Compound Induces Blockage of Cell Proliferation. *J Cell Physiol* **2014,** *229* (11), 1787-1801.

20. Madeira, A.; de Almeida, A.; de Graaf, C.; Camps, M.; Zorzano, A.; Moura, T. F.; Casini, A.; Soveral, G., A Gold Coordination Compound as a Chemical Probe to Unravel Aquaporin-7 Function. *ChemBioChem* **2014,** *15* (10), 1487-1494.
21. de Almeida, A.; Martins, A. P.; Mósca, A. F.; Wijma, H. J.; Prista, C.; Soveral, G.; Casini, A., Exploring the gating mechanisms of aquaporin-3: new clues for the design of inhibitors? *Mol BioSyst* **2016,** *12* (5), 1564-1573.
22. Spinello, A.; de Almeida, A.; Casini, A.; Barone, G., The inhibition of glycerol permeation through aquaglyceroporin-3 induced by mercury(II): A molecular dynamics study. *J Inorg Biochem* **2016,** *160*, 78-84.
23. Mosca, A. F.; de Almeida, A.; Wragg, D.; Martins, A. P.; Sabir, F.; Leoni, S.; Moura, T. F.; Prista, C.; Casini, A.; Soveral, G., Molecular Basis of Aquaporin-7 Permeability Regulation by pH. *Cells* **2018,** *7* (11).
24. de Almeida, A.; Mosca, A. F.; Wragg, D.; Wenzel, M.; Kavanagh, P.; Barone, G.; Leoni, S.; Soveral, G.; Casini, A., The mechanism of aquaporin inhibition by gold compounds elucidated by biophysical and computational methods. *Chem Commun* **2017,** *53* (27), 3830-3833.
25. Graziani, V.; Marrone, A.; Re, N.; Coletti, C.; Platts James, A.; Casini, A., A Multi-Level Theoretical Study to Disclose the Binding Mechanisms of Gold(III)–Bipyridyl Compounds as Selective Aquaglyceroporin Inhibitors. *Chem Eur J* **2017,** *23* (55), 13802-13813.
26. Cattalini, L.; Doni, A.; Orio, A., Reactivity of amines toward cationic gold(III) complexes. *Inorg Chem* **1967,** *6* (2), 280-283.
27. Li, J.; Hu, J.; Gu, Y.; Mei, F.; Li, T.; Li, G., Catalytic activities and properties of Au(III)/Schiff-base complexes in methanol oxidative carbonylation. *J Mol Catal A-Chem* **2011,** *340* (1), 53-59.
28. Yam, V. W.-W.; Choi, S. W.-K.; Lai, T.-F.; Lee, W.-K., Syntheses, crystal structures and photophysics of organogold(III) diimine complexes. *Dalton Trans* **1993,** (6), 1001-1002.
29. Ivanov, M. A.; Puzyk, M. V.; Tkacheva, T. A.; Balashev, K. P., Effect of heterocyclic diimine ligands with donor and acceptor substituents on the spectroscopic and electrochemical properties of Au(III) complexes. *Russ J Gen Chem* **2006,** *76* (2), 165-169.
30. Ahmadi, R.; Amani, V.; Khavasi, H. R., Dichlorido(4,7-diphenyl-1,10-phenanthroline-kappaN,N')gold(III) tetra-chloridoaurate(III). *Acta Crystallogr Sect E Struct Rep Online* **2008,** *64* (Pt 9), m1156-7.
31. Zou, T.; Lum, C. T.; Lok, C.-N.; Zhang, J.-J.; Che, C.-M., Chemical biology of anticancer gold(iii) and gold(i) complexes. *Chem Soc Rev* **2015,** *44* (24), 8786-8801.
32. Aikman , B.; Wenzel, M. N.; Mósca, A. F.; de Almeida, A.; Klooster, W. T.; Coles, S. J.; Soveral, G.; Casini, A., Gold(III) pyridine-benzimidazole complexes as aquaglyceroporin inhibitors and antiproliferative agents. *Inorganics* **2018,** *6*, 123.

33. Wesselinova, D.; Kaloyanov, N.; Dimitrov, G., Cytotoxicity and effects of 1,10-phenanthroline and 5-amino-1,10-phenanthroline derivatives on some immunocompetent cells. *Eur J Med Chem* **2009,** *44* (12), 5099-5102.
34. Roy, S.; Hagen Katharine , D.; Maheswari, P. U.; Lutz, M.; Spek Anthony , L.; Reedijk, J.; van Wezel Gilles , P., Phenanthroline Derivatives with Improved Selectivity as DNA-Targeting Anticancer or Antimicrobial Drugs. *ChemMedChem* **2008,** *3* (9), 1427-1434.

Table of contents synopsis

A series of six new Au(III) coordination compounds with phenanthroline ligands have been synthesized and studied for the inhibition of the water and glycerol channel aquaporin-3 (AQP3). Combining different experimental and computational approaches, further insights into the mechanisms of AQP3 inhibition by gold compounds at a molecular level has been gained. The results evidence the importance of non-coordinative adducts formation, prior to 'covalent' protein binding, to achieve selective AQP3 inhibition.